Analytica Chimica Acta 1203 (2022) 339709

Contents lists available at ScienceDirect

Analytica Chimica Acta

journal homepage: www.elsevier.com/locate/aca

# A novel magnetic molecularly imprinted polymer for selective extraction and determination of quercetin in plant samples

Abdelhafid Karrat [a, b], José María Palacios-Santander [b, *], Aziz Amine [a, **], Laura Cubillana-Aguilera [b]

[a] Laboratory of Process Engineering and Environment, Faculty of Sciences and Techniques, Hassan II University of Casablanca, P.A. 146, Mohammedia, Morocco

[b] Department of Analytical Chemistry, Institute of Research on Electron Microscopy and Materials (IMEYMAT), Faculty of Sciences, Campus de Excelencia Internacional del Mar (CEIMAR), University of Cadiz, Campus Universitario de Puerto Real, Polígono del Río San Pedro S/N, 11510, Puerto Real, Cádiz, Spain

## HIGHLIGHTS

- A new magnetic MIP was prepared using a green ultrasound process.
- Magnetic MIP was combined with fluorometric detection of quercetin (QCT).
- Magnetic MIP-SPE was used for QCT extraction and determination from plant extracts.
- A new paper-based analytical device for smartphone detection of QCT was developed.

## GRAPHICAL ABSTRACT

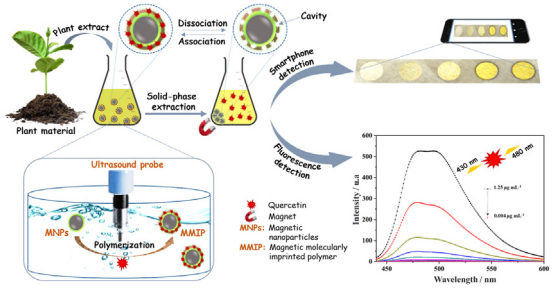


## ARTICLE INFO

*Article history:*
Received 21 January 2022
Received in revised form
7 March 2022
Accepted 8 March 2022
Available online 10 March 2022

*Keywords:*
Molecularly imprinted polymers
Solid-phase extraction
Magnetic nanoparticles
Quercetin
Fluorescence detection
Paper-based analytical device
High energy ultrasound-based synthesis

## ABSTRACT

Molecularly imprinted polymers that mimic the binding mechanism of antibodies and their antigens exhibit several advantages, such as fast synthesis, low cost, high stability, and allow to overcome the ethical issues associated with antibody farming in animals. Herein, a novel strategy combining the magnetic molecularly imprinted polymer (MMIP) as an artificial antibody with a fluorescence procedure for the detection of quercetin in plant samples was designed. The MMIP was synthesized via a radical polymerization process to recognize specific functional groups of quercetin using a green technique based on high energy ultrasound irradiation. The developed MMIP was characterized by Fourier transform infrared spectroscopy, X-ray diffraction, scanning/transmission electron microscopy, and thermal gravimetric analysis, which confirmed the successful preparation of MMIP. The adsorption capacity and selectivity of the MMIP for quercetin and other interferents analogous were performed. The MMIP was applied in the solid-phase extraction (SPE) technique as a selective sorbent for the sample preparation. Besides, a sensitive fluorometric method for the quantitation of quercetin was developed. A linear response was obtained within the concentration of 0.005–1.25 μg $mL^{-1}$ of quercetin. The limit of detection and quantitation were 1.1 ng $mL^{-1}$ and 3.7 ng $mL^{-1}$, respectively. The average recoveries for quercetin were between 92.2% and 104.7% with an RSD less than 5.06% in spiked orange juice and tea extract samples. Furthermore, the developed procedure was successfully combined with a new paper-based analytical device for on-site smartphone analysis of quercetin.



** Corresponding author.
* Corresponding author.
*E-mail addresses:* josem.palacios@uca.es (J.M. Palacios-Santander), azizamine@yahoo.fr (A. Amine).

https://doi.org/10.1016/j.aca.2022.339709

## 1. Introduction

Because of the high increase of chronic diseases (such as cancer and cardiovascular, respiratory and digestive system diseases), which are major causes of death in the world [1], currently, the medical field is focused on the search for new active principles capable of inhibiting such chronic diseases. Plants are considered as real drugs of the above illnesses because they are very rich in bioactive substances [2]. Quercetin (QCT) is a polyphenolic flavonoid richly present in plants including fruits, vegetables, tea, etc. Huge attention to this biomolecule is associated with its high bioactivity. In fact, it exhibits strong antioxidant, anticancer, antiallergic, anti-inflammatory, antiviral and cardioprotective activities [3–7]. Thanks to its properties, QCT is widely used in the medical and pharmaceutical fields. However, its extraction and isolation from the plant extract are extremely difficult. Indeed, the traditional procedures used for the separation and extraction of QCT from the plant extracts were always time-consuming and solvent-dependent [8]. Therefore, the elaboration of a selective, fast, simple and accurate method for the extraction and detection of QCT is highly desired.

Many different methods have been reported for the extraction and determination of QCT, including high pressure liquid chromatography (HPLC) [9,10], spectrophotometry [11,12], luminescence [13], capillary electrophoresis [14], spectrofluorometry [15] and electrochemical sensors [16–19]. These methods provide good experimental results, but tedious sample preparation was required in order to remove the interferents from the sample matrix. Therefore, sample preparation should be performed to isolate the analyte from the sample matrix. Solid-phase extraction (SPE) is a technique that uses a sorbent for the extraction of the target molecule from a given sample [20]. Nevertheless, the majority of the materials used for SPE are not selective to the analyte. To overcome this problem, it is necessary to develop a practicable selective material, such as molecularly imprinted polymers (MIPs). MIPs are artificial antibodies with specific cavities for a template molecule. The MIPs recognize the template molecule by the similar antigen-antibody recognition mechanism in the natural systems [21,22]. MIPs exhibit many advantages, including easy and rapid preparation, low cost and high thermal and chemical stability [23,24]. Recently, MIPs have received great attention and have been effectively employed for selective extraction, determination and pre-concentration of several target molecules including quercetin. Indeed, Rahimi et al. [10] developed a molecularly imprinted polymer combined with high-performance liquid chromatography for the determination of quercetin. The sol-gel process was used for the preparation of the MIP. The developed method presented a detection limit of 9.94 ng $mL^{-1}$ and it was successfully applied for the determination of QCT in tea and coffee samples. Moreover, Sun et al. [25] reported an electrochemical sensor based on MIP, polypyrrole, and graphene oxide for the selective determination of quercetin in fruit juices. The MIP was formed by electropolymerization using pyrrole as a functional monomer and graphene oxide to improve the electron transfer rate. The developed sensor provided a linear range of 0.181–4.53 μg $mL^{-1}$ and a detection limit of 14.50 ng $mL^{-1}$. Furthermore, MIPs have been extensively employed in the dispersive SPE technique in order to enhance its selectivity and to reduce the consumption of organic solvents, extraction time and amount of sorbent [26,27]. Besides, the application of the magnetic nanoparticles as core materials of MIP facilitates the separation and recovery of MIP after the solid-phase extraction process [28–30].

Chitosan is a biopolymer obtained by deacetylation of chitin. Chitosan has been largely used for the development of MIPs thanks to its properties including film forming ability, biodegradability and non-toxicity [31–33].

It was previously reported that the synthesis of MMIPs based on the use of a high-power ultrasound probe is a green technology for the synthesis of materials and presents many beneficial advantages in comparison to other techniques including thermal heating, photo-polymerization, ultrasonic bath, and microwave irradiation. Acceleration of polymerization reaction rate, reducing energy consumption, production of more homogenous polymer chains, and degassing property are the mains advantages of ultrasound technique [34].

The development of paper-based analytical devices (PADs) for the rapid, on-site detection of multiple molecules is of great interest in various fields, including environmental monitoring, food safety, disease diagnosis, etc [35,36]. However, the majority of PADs exhibits poor selectivity. The combination of SPE using MIP with PAD allows a rapid and selective determination of the target molecule.

In this study, a magnetic molecularly imprinted polymer (MMIP) was synthesized by radical polymerization of the monomer promoted by ultrasound irradiation and in the presence of QCT as a template.

Magnetic nanoparticles were employed as core material and chitosan was used as dispersive agent and to link the polymethacrylic acid with the magnetic nanoparticles. The adsorption and the analytical characteristics of the MMIP toward QCT were performed. Then, a sensitive fluorometric method for the trace detection of QCT was developed. The synthesized MMIP was effectively combined with the spectrofluorometric method for the selective extraction and detection of QCT in plant samples.

## 2. Experimental part

### 2.1. Material

Methacrylic acid (MAA) 99%, QCT, ammonium hydroxide ($NH_4OH$), ethylene glycol dimethacrylate (EGDMA) 98%, chitosan, ferric chloride hexahydrate ($FeCl_3 \cdot 6H_2O$), ammonium persulfate (APS) ≥ 98%, and ferrous chloride tetrahydrate ($FeCl_2 \cdot 4H_2O$) were purchased from Sigma Aldrich (Spain). Methanol 99.9% and dimethylsulfoxide (DMSO) 99% were purchased from PanReac (Spain). Nanopure water (18 MΩ cm) was obtained from a Millipore Milli-Q system (Bedford, MA, USA).

### 2.2. Instrumentation

A high-power ultrasound probe generator SONICATOR 4000 (Misonix Inc., Farmingdale, NY, USA), which operates at 20 KHz and provides a maximum power of 700 W, equipped with a 13 mm diameter titanium tip, was used for the synthesis of MMIP. A double beam UV/vis spectrophotometer, model T80+ from PG Instruments (Leicestershire, England), with 1 nm resolution, was used for the evaluation of the adsorption capacities of the developed MMIP and MNIP. Fourier transform infrared (FT-IR) spectra were collected using a IR Affinity-1S SHIMADZU spectrophotometer, in the Attenuated Total Reflectance (ATR) mode and in the range of 4000–500 $cm^{-1}$. X-ray diffraction measurements were recorded on a Bruker D8 Advance A25 X-ray diffractometer (BRUKER-AXS, Germany), equipped with a LINXEYE detector and Cu-Kα radiation source (λ = 0.1542 nm). Scanning-transmission electron microscopy (STEM) images were obtained by a FEI Nova NANOSEM 450 equipment (Thermo Fisher Scientific, USA) (resolution = 1 nm). Thermo-gravimetric analyses (TGA) data were carried out on a TGA Q50 V20.13 Build 39 from TA Instruments (Delaware, USA) via heating from 30 °C until 800 °C, at a rate of 10 °C/min under nitrogen:air (4:6 v/v) flow. Finally, a FP-6500 spectrofluorometer (Jasco, Spain) was used for the determination of QCT.

### 2.3. Synthesis of $Fe_3O_4$-Chitosan

$Fe_3O_4$-Chitosan was synthesized according to the process reported by Lui et al. [37]. 0.25% (w/v) of chitosan was prepared in acetic acid solution (0.25%; v/v). The obtained chitosan solution was added to 20 mL of a mixture containing 0.3 g of $FeCl_2{\cdot}4H_2O$ and 0.7 g of $FeCl_3{\cdot}6H_2O$ under mechanical stirring (800 rpm). After complete dissolution (1 h), 15 mL of $NH_4OH$ was added drop by drop under stirring for the next 30 min. The obtained $Fe_3O_4$-chitosan nanoparticles were recovered and washed with distilled water to neutral pH and cured at 60 °C.

### 2.4. Preparation of MMIP-coated $Fe_3O_4$-Chitosan

MIP-coated $Fe_3O_4$-Chitosan was prepared according to the method reported in our previous work [38] (Scheme 1), using MAA, EGDMA, QCT and APS as monomer, cross-linking agent, template and initiator, respectively. 172 μL of MAA and 67.5 mg of QCT were dispersed in 10 mL of DMSO; the mixture was incubated at 3 °C for 1 h to facilitate the combination between the template and the monomer. Then, 40 mL of DMSO:water (1:3 v/v) containing 100 mg of $Fe_3O_4$-chitosan nanoparticles, 317 μL of EGDMA and 40 mg of APS were added to the above solution. The blend was deaerated with nitrogen for 15 min and the reaction was carried out at 60 °C for 40 min, using the high-power ultrasound probe at an amplitude of 30%. Then, the MMIP was collected using a magnet and washed several times with an acetic acid:methanol (1:9, v/v) solution until QCT was not detected by UV spectrophotometer. Simultaneously, magnetic non-imprinted polymers (MNIP) were developed identically except for the addition of QCT.

### 2.5. Binding experiments

To perform the binding isotherm experiments, 1 mg of MMIP or MNIP was introduced into QCT solutions prepared in Milli-Q water (2 mL) at different concentrations ranging from 10 to 30 μg $mL^{-1}$. The solutions were shacked for 5 min at ambient temperature and subsequently separated by a magnet. The obtained QCT supernatant was analyzed with the spectrophotometer at the wavelength of 402 nm. For the binding kinetic experiments, 1 mg of MMIP was suspended in 2 mL of QCT (10 mg $L^{-1}$) and shacked at 600 rpm for measuring the adsorption capacity as a function of time.

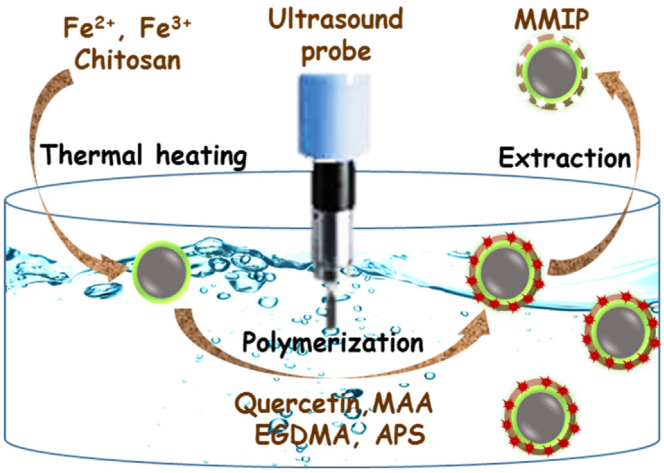


**Scheme 1.** Ultrasound preparation of magnetic molecularly imprinted polymers (MMIP); EGDMA: Ethylene glycol dimethacrylate, MAA: Methacrylic acid, APS: Ammonium persulfate.

The uptake capacities of MMIP to QCT were defined by $Q$ ($mg{\cdot}g^{-1}$) (Eq. (1)):

$$Q = \frac{C_i - C_e}{m} V \tag{1}$$

where $C_i$ ($\mu g{\cdot}mL^{-1}$) is the initial concentration of QCT; $C_e$ is the QCT equilibrium concentration; $V$ (mL) is the volume of the QCT solution; and $m$ (g) is the mass of MMIP and MNIP.

The adsorption equilibrium data were fitted to Langmuir and Freundlich isotherm models. The equations were illustrated as follows:

Freundlich equation (Eq. (2)):

$$\text{Log } Q_e = \frac{1}{n} \text{Log } C_e + \text{Log } K_f \tag{2}$$

where $n$ and $K_f$ are the Freundlich isotherm parameters related to the intensity and the adsorption capacity, respectively.

Langmuir equation (Eq. (3)):

$$\frac{C_e}{Q_e} = \frac{1}{Q_m \cdot K_L} + \frac{C_e}{Q_m} \tag{3}$$

where $Q_e$ ($mg{\cdot}g^{-1}$) is the equilibrium uptake capacity; $C_e$ ($\mu g{\cdot}mL^{-1}$) is the equilibrium analyte concentration; $Q_m$ is the maximum uptake capacity of the MMIP, and $K_L$ is the Langmuir constant.

The kinetic data was analyzed using pseudo-first order (PFO) (Eq. (4)) and pseudo-second-order (PSO) (Eq. (5)) rate models.

$$\log(Q_e - Q_t) = \log(Q_e) - \frac{k_1}{2,303} t \tag{4}$$

$$\frac{t}{Q_t} = \frac{1}{k_2 Q_e^2} + \frac{t}{Q_e} \tag{5}$$

where $Q_t$ ($mg{\cdot}g^{-1}$) is the binding capacity at time $t$ (min); $Q_e$ ($mg\ g^{-1}$) is the binding capacity at the equilibrium concentration; and $k_1$ ($min^{-1}$) and $k_2$ ($g{\cdot}mg^{-1}{\cdot}min^{-1}$) are the rate constants of the PFO and PSO, respectively.

For the selectivity study, 1 mg of MMIP or MNIP was introduced into 2 mL of solutions containing 33 μM of either QCT or caffeic acid, rutin or ferulic acid used as the structural analogous. After the adsorption and separation steps, the supernatant of the tested molecules QCT, caffeic acid, rutin and ferulic acid were measured by spectrophotometry at their corresponding maximum absorbance wavelengths of 402, 326, 375 and 330 nm, respectively.

To evaluate the selectivity efficiency of the proposed MMIP, a selectivity factor ($\alpha$) was determined from the following formula (Eq. (6)):

$$\alpha = \frac{Q_{QCT}}{Q_{analog}} \tag{6}$$

where $Q_{QCT}$ and $Q_{analog}$ are the adsorption capacities of QCT and the structural analogous molecules, respectively.

### 2.6. Solid-phase extraction experiment

The solid-phase extraction of QCT using MMIP as a sorbent was investigated as follows: 2 mg of MMIP were added into 2 mL of QCT aqueous solution; later, the blend was shaked for 15 min at 25 °C. After the separation with the magnet, the MMIP was eluted by 2 mL of methanol. Finally, the desorbing solution was analyzed by UV/vis spectrophotometry.

### 2.7. Determination of QCT

#### 2.7.1. Spectrophotometric and fluorometric detection

QCT can be measured directly at their maximum absorbance of 402 nm. However, in the presence of aluminum, the absorbance drastically increases. The procedure is based on the addition of 10 μL of $AlCl_3$ (10%) to 2 mL of methanol containing QCT. The obtained complex (QCT-Al) was analyzed either with a spectrophotometer at $\lambda = 451$ nm or with a spectrofluorometer under the excitation wavelength of 430 nm and the emission wavelength of 480 nm.

#### 2.7.2. Paper-based analytical device

A new paper-based analytical device (PAD) was applied for the smartphone determination of QCT using the following procedure. Firstly, a circle of 1 cm (in diameter) was designed on a Josef paper using the wax pencil in order to have a hydrophobic circumference. Secondly, the device was placed in the oven at 60 °C to dissolve the wax across the paper to create a three-dimensional hydrophobic circumference. In the designated circle, 2 μL of $AlCl_3$ (0.5%) was dropped and dried at ambient temperature. Then, 20 μL of the sample was added onto the prepared circle. The developed color was measured with a smartphone.

### 2.8. Determination of QCT in real samples

Samples of orange juice and tea extract were obtained from a local market. Both samples were spiked with 0.5 and 1 μg $mL^{-1}$ of QCT. Then, 2 mg of MMIP was introduced into 2 mL of the prepared samples and followed by stirring for 15 min. After the separation step, the analyte was extracted by methanol. Then, the supernatant was measured by a fluorometer after forming the complex product with aluminum.

For the determination of QCT in a grape sample, 20 g of grapes were mixed and filtered to remove particulate impurities. After the SPE steps using MMIP as sorbent, the QCT concentration was measured by the developed PAD.

### 2.9. Statistical analysis

The one-way analysis of variance (ANOVA) was used to carry out the statistical analysis. The significant differences between recovery values were considered when $p < 0.05$.

## 3. Results and discussion

### 3.1. Characterization studies

The functional groups of $Fe_3O_4$, $Fe_3O_4$-chitosan and MMIP were characterized by FT-IR (Fig. 1a.). The characteristic peak of Fe−O groups appeared at the wavelength of 549 $cm^{-1}$ in all spectra. For $Fe_3O_4$-chitosan, the peak at 3340 $cm^{-1}$ is assigned to the stretching vibrations of amine (−$NH_2$) and hydroxide (−OH) groups, and the typical peaks of the −$CONH_2$ groups appeared at 1643 $cm^{-1}$, which proves the good modification of $Fe_3O_4$ with chitosan. After the decoration of $Fe_3O_4$-chitosan with MIP, the characteristic peaks of polymethacrylic acid appeared at 1726 and 1157 $cm^{-1}$, matching to C═O and C−O groups, respectively. These results confirm the successful preparation of the MMIP.

The prepared products are further characterized by XRD technique. In Fig. 1b six typical diffraction peaks for $Fe_3O_4$ are obtained in all samples at 2θ values of 30.34°, 35.58°, 43.26°, 53.8°, 57.3° and 62.68°. These peaks were indexed respectively to the following planes (2 2 0), (3 1 1), (4 0 0), (4 2 2), (5 1 1) and (4 4 0). The quoted peaks corresponded well with the standard XRD data of magnetic $Fe_3O_4$ (JCPDS No. 85-1436) [39]. The obtained results showed that the structure of the magnetic nanoparticles throughout the samples stayed unchanged during the polymerization process. Furthermore, the intensity sharpness of the peaks indicated that the MMIP had been successfully designed.

The thermo-gravimetric analysis (TGA) was performed in order to investigate the thermal stability of the three developed materials ($Fe_3O_4$, $Fe_3O_4$-chitosan and MMIP). As illustrated in Fig. 1c, from 250 °C to 450 °C, the weight of $Fe_3O_4$, $Fe_3O_4$-chitosan and MMIP decreased, with 3.86%, 44.1%, and 84% of losses, respectively. The loss in mass means that the chitosan and MIP modified the surface of the $Fe_3O_4$ effectively. However, above 450 °C no significant mass loss was observed, showing that only the thermal resistant $Fe_3O_4$ nanoparticles remained.

STEM was applied for the characterization of the size and the morphological structure of the prepared materials ($Fe_3O_4$, $Fe_3O_4$−chitosan and MMIP). The size of the developed products increased with a mean diameter of about 12.0 ± 2.6 nm (n = 20) (Figs. 1d), 28.0 ± 5.2 nm (n = 20) (Figs. 1e), 76.1 ± 12.1 nm (n = 20) (Fig. 1f) for $Fe_3O_4$, $Fe_3O_4$-chitosan and MMIP, respectively. These results confirm well that magnetic nanoparticles were successfully modified with chitosan and MIP.

### 3.2. Adsorption isotherm

The binding isotherms of QCT on the MMIP and MNIP at 25 °C are presented in Fig. 2a. The binding capacities of the MMIP and MNIP rose with the increment of QCT concentration. Clearly, MMIP presented high adsorption capacity than MNIP thanks to the numerous specific cavities of QCT contained in the MMIP surface. In addition, the imprinted factor, defined as the ratio of the adsorption capacity of MMIP and MNIP, ranged its values between 2.0 and 3.3, which are higher than those obtained in most of the previous published works [40−42]. These results confirm the creation of QCT cavities on the surface of MMIP. Moreover, the adsorption mechanisms of QCT implicate hydrogen bonds between QCT and the functional groups of the monomer.

Freundlich and Langmuir's models were applied to analyze the sorption data of MMIP and MNIP (Fig. S1). As shown in Table S1, the Freundlich regression coefficients ($R^2_{MMIP} = 0.993$; $R^2_{MNIP} = 0.994$) were higher than those obtained with Langmuir model ($R^2_{MMIP} = 0.990$; $R^2_{MNIP} = 0.858$), indicating that the equilibrium data fitted better with Freundlich isotherm model than with Langmuir model, demonstrating that the binding of QCT by this technique implied the multimolecular layer adsorption. Moreover, the Freundlich constant ($K_F$) for QCT on the MMIP was higher than that on the MNIP (Table S2), indicating the stronger affinity of the MMIP for QCT.

### 3.3. Kinetic adsorption

Fig. 2b illustrates the kinetic adsorption of QCT (10 μg $mL^{-1}$) on the MMIP and MNIP. Indeed, the adsorption of QCT by MMIP and MNIP was very fast and reaches the maximum in 15 min. Moreover, the binding capacity of MMIP for QCT was higher than that of MNIP, indicating the high imprinting effect of the MMIP toward QCT. According to the correlation coefficient ($R^2$) described in Table S3, the kinetic data fitted better with the PSO model than the PFO one. The result indicates that the adsorption process of QCT on the MMIP was dominated by chemical sorption and the adsorption capacity was proportional to the number of cavities on the MMIP.

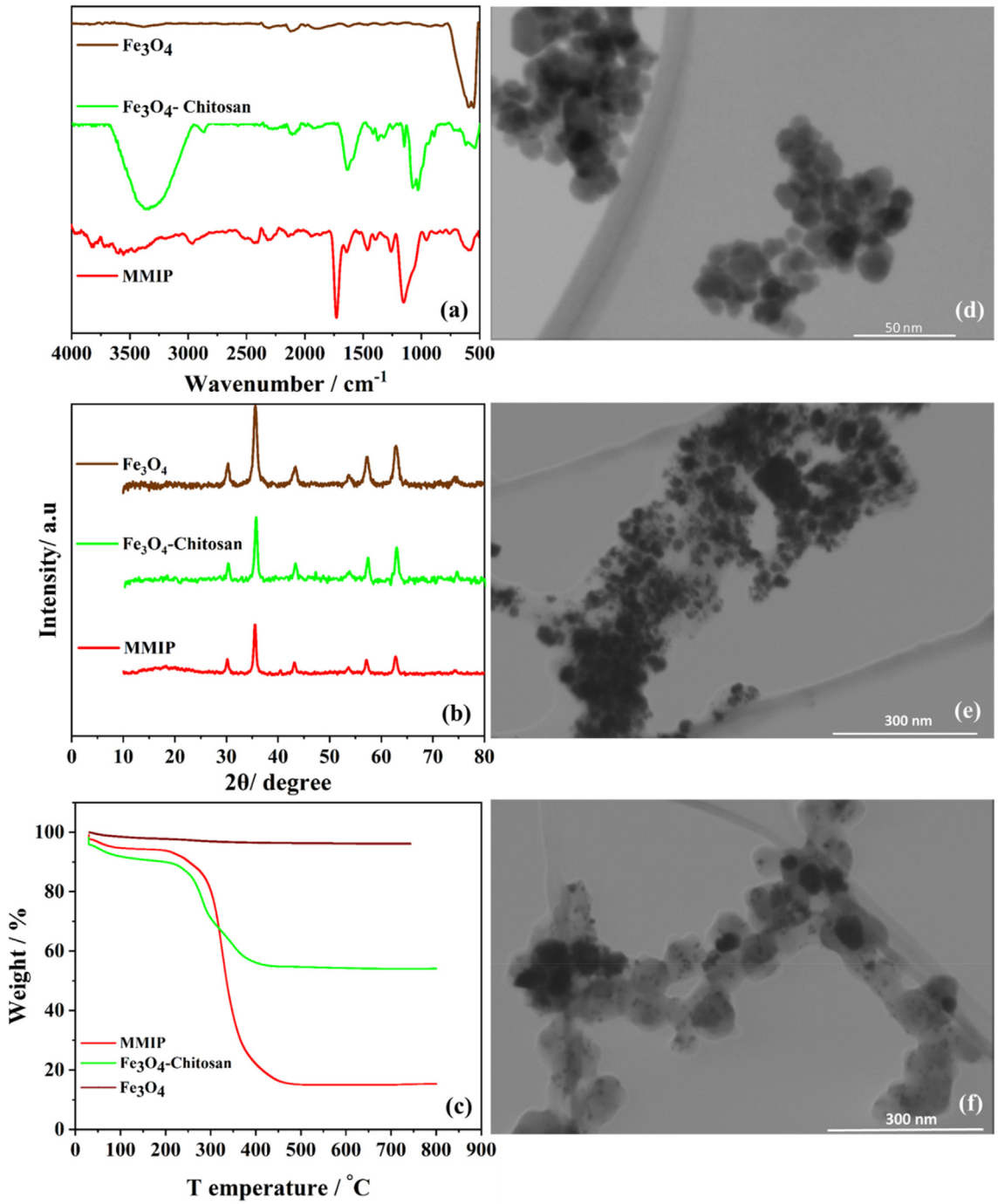


**Fig. 1.** (a) FT-IR spectra; (b) XRD diffractogram and (c) thermo-gravimetric analysis spectra of $Fe_3O_4$, $Fe_3O_4$-chitosan and MMIP. (d), (e), and (f) STEM images of $Fe_3O_4$, $Fe_3O_4$-chitosan and MMIP, respectively.

### 3.4. Selectivity study

The selectivity of the MMIP toward QCT was estimated using similar structural compounds including caffeic acid, rutin and ferulic acid at the concentration of 33 μM. As presented in Fig. 2c., the MMIP has higher binding capacity for QCT compared with caffeic acid, rutin and ferulic acid. Furthermore, the MMIP binding for the interfering molecules was not significantly different from that of MNIP. In addition, the MMIP exhibited a high $\alpha$-factor toward QCT than the other interferents (Table S4) because its structure is complementary in size, shape and functional groups to the cavities of MMIP.

### 3.5. Solid-phase extraction

#### 3.5.1. Type of eluent

In order to obtain the highest elution recovery, the choice of the appropriate solvent is relevant. Two milliliters of solvent, including methanol, ethyl acetate, methanol-water (1:1) and acetone were investigated for eluting the analyte from the MMIP. Fig. 3a demonstrates that methanol has good elution ability than other solvents due to its high polarity and affinity toward QCT. Moreover, the statistical analysis showed that this difference was significant ($p < 0.05$). Thus, methanol was used as elution solvent in the subsequent experiments.

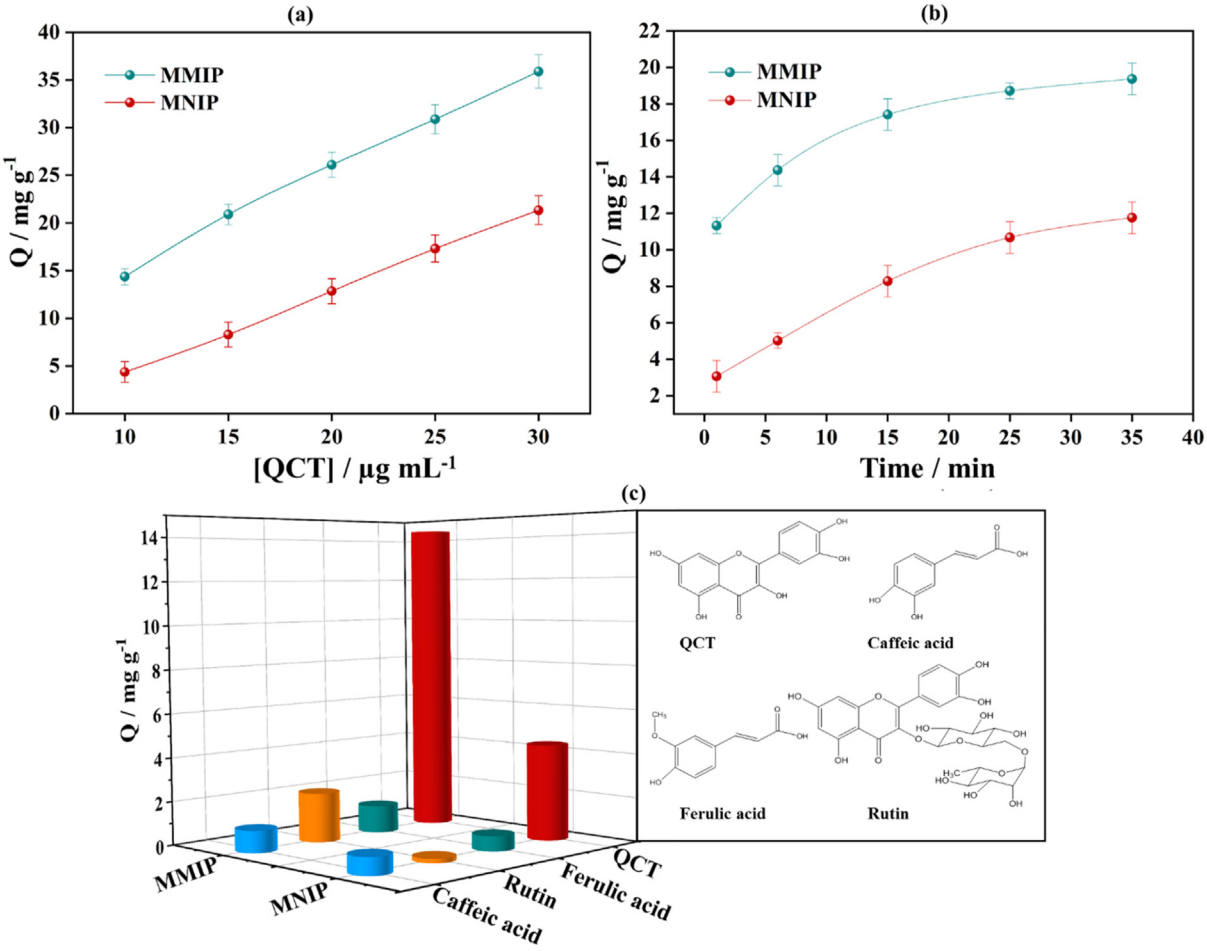


**Fig. 2.** (a) Binding isotherms of QCT on MMIP and MNIP at room temperature; (b) kinetic adsorption of MMIP and MNIP at room temperature and QCT initial concentration ($C_i$): 10 µg mL$^{-1}$; (c) (left) selectivity of MMIP and MNIP for different analytes at room temperature ($C_i$: 10 µg mL$^{-1}$) and (right) chemical structures of the analogous molecules.

*3.5.2. Effect of MMIP concentration*

Various concentrations of MMIP varying from 0.025 to 2 mg mL$^{-1}$ were tested to achieve the optimum recovery (Fig. 3b). The recovery increased significantly ($p < 0.05$) with the MMIP concentration up to 1 mg mL$^{-1}$. After this amount, sorption efficiency decreased slightly and no significant difference was found after 1 mg mL$^{-1}$ according to ANOVA results. Therefore, the optimum MMIP concentration was fixed at 1 mg mL$^{-1}$.

*3.5.3. Effect of elution time*

After determining the optimal eluent solvent and the concentration of MMIP, the time of elution was optimized in the interval from 1 to 20 min (Fig. 3c). The extraction recovery increased significantly ($p < 0.05$) with the extraction time from 1 to 5 min and, after that, stayed almost at a steady-state with a slight reduction ($p > 0.05$), indicating that the analyte was completely removed from the MMIP after 5 min. Therefore, 5 min was selected for the following experiments.

*3.6. Analytical determination of quercetin*

*3.6.1. Spectrophotometric detection*

The reaction of QCT with the aluminum cation leads to the formation of a complex with yellow coloration that absorbs at 451 nm. A regression equation in the linear range of 0.5–10 µg mL$^{-1}$ was obtained: $y = 0.13 \pm 0.003$ [QCT] (µg·mL$^{-1}$) – $0.02 \pm 0.004$ (Standar devia with a regression coefficient of $R^2 = 0.999$.

*3.6.2. Detection of QCT using paper-analytical device*

Paper-based analytical device presents several advantages such as rapidity, easiness, low cost and less toxicity [36]. The detection of QCT using the developed PAD was performed in the concentration range of 10–80 µg mL$^{-1}$. As the concentration of QCT increases (Fig. 4a.), the color intensity of the circle changes from light yellow to dark yellow. Furthermore, an Android-type smartphone (Resolution: 13 MP, 4:3) was used for capturing the images of the developed colored circles. Indeed, Fig. S3 Showed that the intensity of the blue color decreases more significantly with the increase of QCT concentration than the green and red colors. Therefore, we selected the blue color as the optimal parameter for the determination of QCT using ImageJ software. The PAD as proposed would be useful for the rapid quantitation of QCT in plants rich in this flavonoid such as cranberries and grapes [43,44]. Indeed, the developed PAD was successfully used for determination of QCT in grape sample (Fig. S4).

*3.6.3. Fluorometric determination*

The PAD method allows rapid on-site detection of QCT, but it is not highly sensitive for the determination of QCT in plants containing low concentrations of QCT substance such as apple (20–42.6 ng mL$^{-1}$), onion 30-190 ng mL$^{-1}$, pepper 107.6 ng mL$^{-1}$, etc [45,46]. For this reason, we have applied the same procedure based

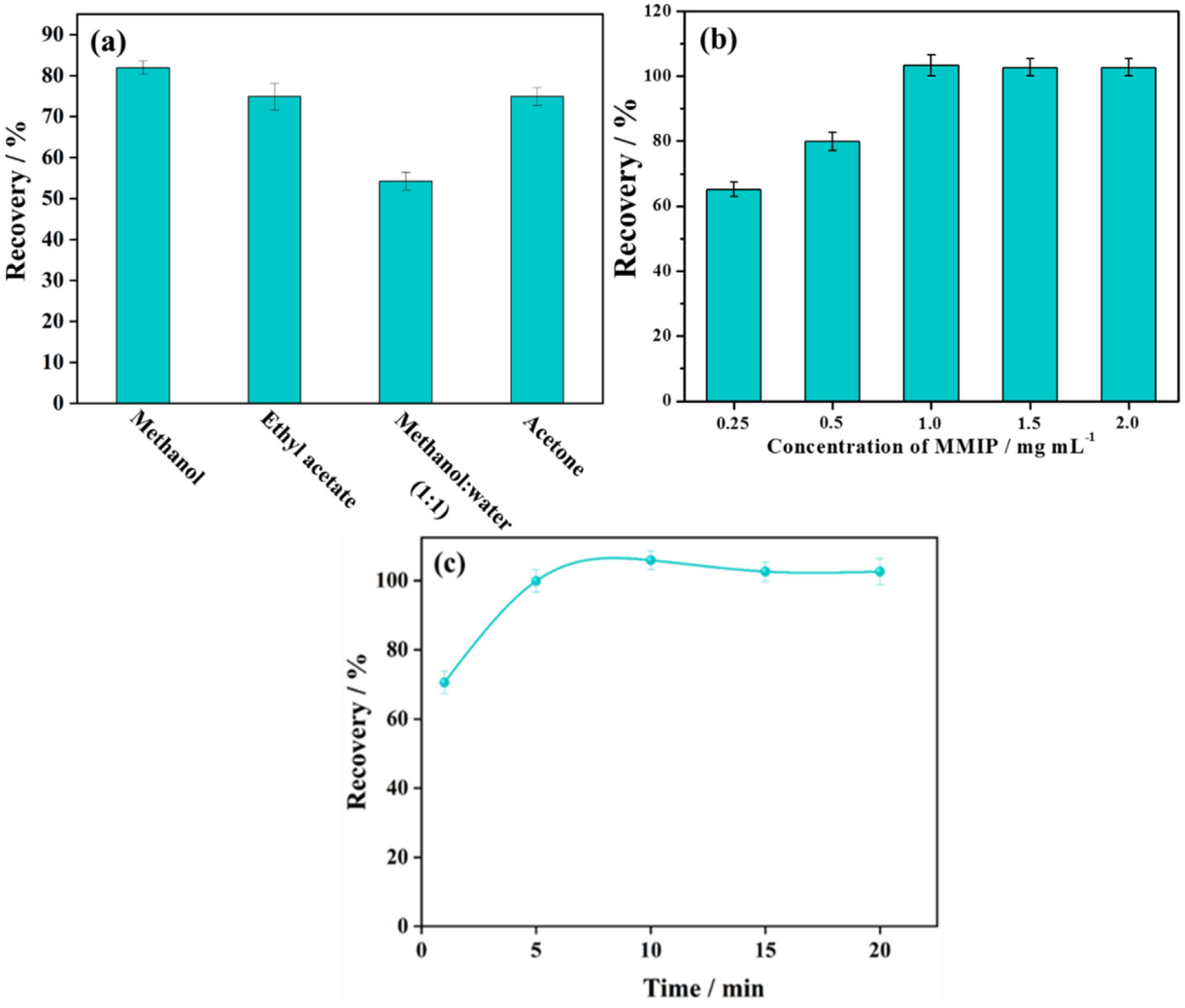


**Fig. 3.** Effect of extraction conditions on QCT recovery at room temperature: (a) eluent solvent; (b) MMIP concentration; and (c) elution time.

on the QCT complexation with the aluminum ion for fluorometric detection. A calibration curve was achieved (Fig. 4c) within the wide concentration range of 0.005–1.25 μg $mL^{-1}$ of QCT. The linear regression equation was y = 222.6 ± 3.0 [QCT] ($\mu g \cdot mL^{-1}$) + 1.2 ± 0.37 ($R^2$ = 0.999). Based on the calibration curve, the calculated limit of detection LOD was 1.1 ng $mL^{-1}$ (LOD = 3·SD/slope) and the limit of quantitation was 3.7 ng $mL^{-1}$ (LOQ = 10·SD/slope). These findings confirmed that the developed fluorometric method provides prospective advantages including high sensitivity, simplicity and fastness for the QCT detection. It is worth noting that this fluorometric procedure based on the complexation of QCT with aluminum is traditionally recommended for aluminum determination [47]. However, in this work, we succeeded to apply it for quercetin determination.

### 3.7. Real samples

To demonstrate the feasibility and reliability of the proposed procedure, the proposed methodology was employed for the detection of QCT in spiked orange juice and tea extract samples. As depicted in Table 1, the average QCT recoveries in both real samples ranged from 92.2% to 104.7% and the RSD values were between 1.50 and 5.1%. The obtained results demonstrated that the developed procedure provided good precision and accuracy. Therefore, this methodology would be useful for monitoring QCT in food samples.

In addition, Table 2 presents a comparative study of the proposed methodology with other procedures previously reported in the literature. It can be concluded that the proposed method has high sensitivity as well as wide linear range for the determination of QCT. Furthermore, as mentioned in the introduction, QCT is a very interesting biomolecule thanks to its biological properties. Thus, its selective extraction and its determination in plant samples are in high demand. The procedure described in this work has confirmed well its ability to selectively extract QCT from complex plant extracts using the developed synthetic antibody and to determine it with high sensitivity using the fluorometric method.

### 3.8. Reusability

For assessing the reusability of the proposed MMIP, adsorption and desorption assays of QCT from MMIP were performed 5 times successively. This experience was repeated with three different MMIPs. The results showed no significant loss of recovery (90.6–99.8%) as presented in Fig. S5.

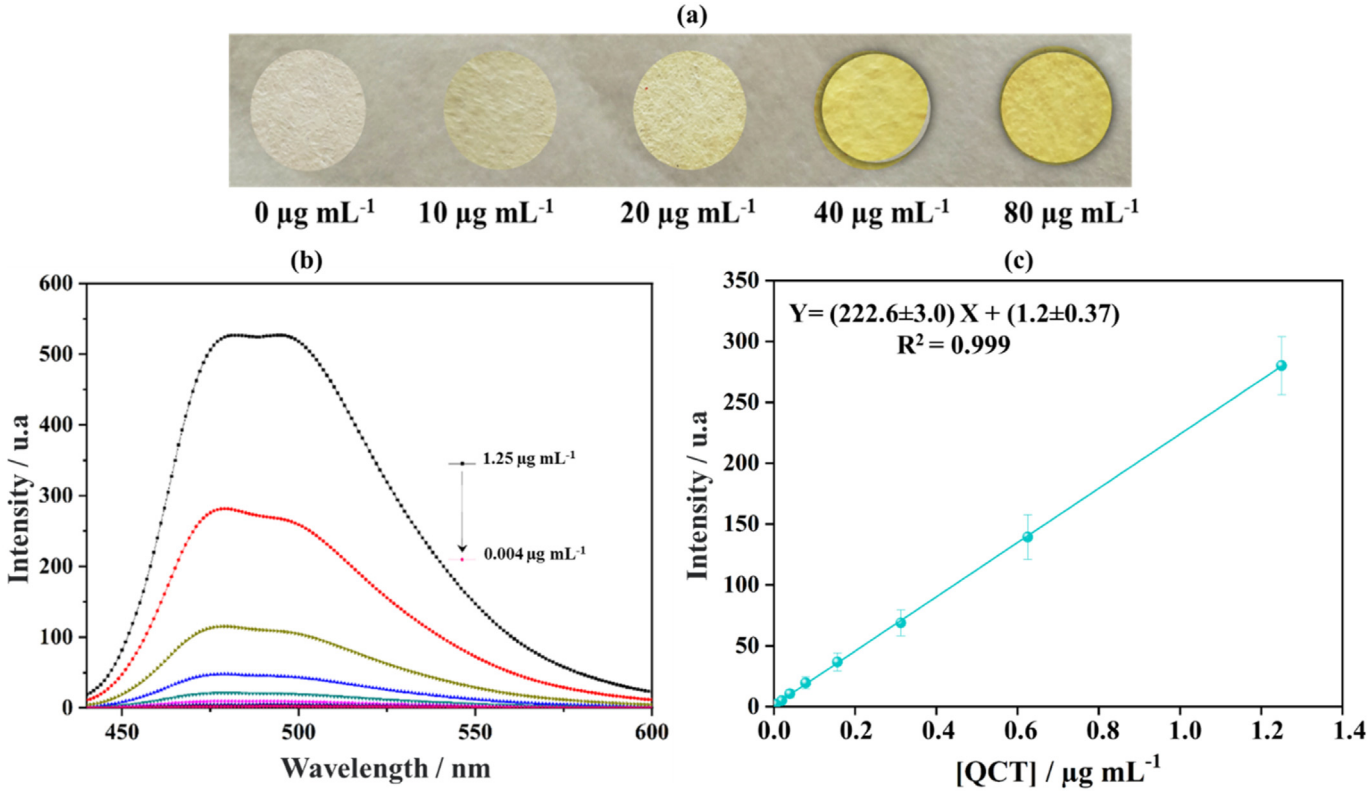


**Fig. 4.** (a) Detection of QCT using the developed PAD; (b) Fluorescence spectra of quercetin; (c) calibration curve for quercetin determination at room temperature; $\lambda_{ex}$ = 430 nm and $\lambda_{em}$ = 480 nm. Final aluminum concentration = 0.05%.

**Table 1**
Determination of QCT in orange juice and tea extract samples by MMIP coupled with spectrofluorimetry.

| Sample | Added ($\mu g \cdot mL^{-1}$) | Found ($\mu g \cdot mL^{-1}$) | Recovery (%) | RSD (n = 3) |
|---|---|---|---|---|
| Orange juice | 0 | 0.081 | – | – |
| | 0.5 | 0.572 | 98.2 | 2.2 |
| | 1 | 1.128 | 104.7 | 1.8 |
| Tea extract | 0 | 0.052 | – | – |
| | 0.5 | 0.507 | 92.2 | 1.5 |
| | 1 | 1.028 | 97.7 | 5.1 |

**Table 2**
Comparison of the proposed procedure with other reported methods in the literature.

| | Linear range ($\mu g \cdot mL^{-1}$) | LOD ($ng \cdot mL^{-1}$) | Recovery (%) | Advantages/disadvantages of the reported method | Ref |
|---|---|---|---|---|---|
| MIP-GO-GC | 0.181–4.53 | 14.50 | 97.4 –101.4 | Low sensitivity, good stability, and repeatability. | [25] |
| MIP-SPME-HPLC-UV | 0.05–100 | 9.94 | 94.2–98.5 | Long synthesis time (12 h), and complicated preparation method, high selectivity. | [10] |
| MIP-MSPD | 1–500 | 250 | 102.3 | Long synthesis time (26 h), low imprinting factor, fast adsorption, low sensitivity. | [40] |
| SPE-HPLC-UV | – | 60 | 41.7 | Able to detect a larger number of phenolic acids and flavonols polyphenols, low sensitivity. | [48] |
| MISPE | 0.01–0.1 | 2.6 | – | Low imprinting factor (1.42), Long rebinding time (12 min), low limit of detection, | [49] |
| DLLME-SFOD | 0.015–0.15 | 3.02 | 95.0 –105.0 | Consumption of organic solvents, complicated extraction steps, good recovery | [50] |
| MMIP-Fluorescence | 0.005–1.25 | 1.1 | 92.2 –104.7 | Rapid synthesis method, fast adsorption, high selectivity and sensitivity, good repeatability, easy sorbent recovery | This work |

GO: Graphene oxide; GC: Glassy carbon electrode; SPME: Solid-phase microextraction; HPLC-UV: high-performance liquid chromatography with UV detection; MSPD: Matrix solid-phase dispersion; MISPE: Molecularly imprinted solid-phase extraction; SPE: Solid-phase extraction procedure; DLLME: Dispersive liquid-liquid microextraction; SFOD: Solidification of floating organic drop; MMIP: Magnetic molecularly imprinted polymer.

## 4. Conclusions

In this work, a new MMIP was successfully developed to facilitate the extraction and determination of quercetin in plant samples. The green technique based on high energy ultrasound irradiation allowed a rapid synthesis of MMIP. Also, the characterization results (using FTIR, XRD, TGA, and TEM) confirmed the successful preparation of MMIP. Effectively, the developed MMIP was

combined with the fluorometric method for the selective solid-phase extraction and sensitive determination of QCT. Indeed, a very good sensitivity and selectivity toward QCT were obtained. Moreover, the recoveries of QCT from spiked orange juice and tea extract were in the range of 92.2% and 104.7%. In addition, the proposed MMIP was successfully coupled with the developed PAD for on-site smartphone analysis of QCT.

Furthermore, the advantages of the developed MMIP including high selectivity, easiness and rapid preparation, low-cost and good stability confirmed well that MIPs could be used as outstanding synthetic antibodies for the development of novel biosensors in the determination of several analytes in plant samples.

## CRediT authorship contribution statement

**Abdelhafid Karrat:** Conceptualization, Investigation, Methodology, Formal analysis, Writing – original draft, Validation. **José María Palacios-Santander:** Supervision, Funding acquisition, Project administration, Writing – review & editing. **Aziz Amine:** Supervision, Conceptualization, Project administration, Writing – review & editing. **Laura Cubillana-Aguilera:** Funding acquisition, Resources, Writing – review & editing, Visualization.

## Declaration of competing interest

The authors declare that they have no known competing financial interests or personal relationships that could have appeared to influence the work reported in this paper.

## Acknowledgments

The authors thank Junta de Andalucia (PAIDI2020), Institute of Research on Electron Microscopy and Materials (IMEYMAT, Polybiosens project), and Programa de Fomento e Impulso de la Investigación y de la Transferencia de la Universidad de Cádiz 2020-2021 for the project PR2020-013 (Proyectos de Investigación-Puente 2020). Authors also acknowledge Ms. María del Rocío González-Moya (Technician of the University of Cadiz, Spain) for her assistance in performing the TGA analyses, and Electron Microscopy and XRD Divisions from Servicios Centrales de Investigación Científica y Tecnológica of University of Cadiz (SC-ICYT-UCA) for their technical assistance during STEM and XRD measurements. Finally, authors thank TEP-243 research group for the help given to register the ATR-FTIR spectra.

This work was supported by EU-PRIMA-FEDKITO project - Fresh food sustainable packaging in the circular economy.

## Appendix A. Supplementary data

Supplementary data to this article can be found online at https://doi.org/10.1016/j.aca.2022.339709.

## References

[1] M.C. Garcia, L.M. Rossen, B. Bastian, M. Faul, N.F. Dowling, C.C. Thomas, L. Schieb, Y. Hong, P.W. Yoon, M.F. Iademarco, Potentially excess deaths from the five leading causes of death in metropolitan and nonmetropolitan counties — United States, 2010–2017, MMWR Surveill. Summ. 68 (2019) 1–11, https://doi.org/10.15585/mmwr.ss6810a1.

[2] M. Diederich, Natural products target the hallmarks of chronic diseases, Biochem. Pharmacol. 173 (2020) 113828, https://doi.org/10.1016/j.bcp.2020.113828.

[3] Q. Tang, F. Ji, J. Wang, L. Guo, Y. Li, Y. Bao, Quercetin exerts synergetic anticancer activity with 10-hydroxy camptothecin, Eur. J. Pharmaceut. Sci. 109 (2017) 223–232, https://doi.org/10.1016/j.ejps.2017.08.013.

[4] M. Lesjak, I. Beara, N. Simin, D. Pintać, T. Majkić, K. Bekvalac, D. Orčić, N. Mimica-Dukić, Antioxidant and anti-inflammatory activities of quercetin and its derivatives, J. Funct.Foods 40 (2018) 68–75, https://doi.org/10.1016/j.jff.2017.10.047.

[5] E. Escribano-Ferrer, J. Queralt Regué, X. Garcia-Sala, A. Boix Montañés, R.M. Lamuela-Raventos, *In vivo* anti-inflammatory and antiallergic activity of pure naringenin, Naringenin chalcone, and quercetin in mice, J. Nat. Prod. 82 (2019) 177–182, https://doi.org/10.1021/acs.jnatprod.8b00366.

[6] G. Wong, S. He, V. Siragam, Y. Bi, M. Mbikay, M. Chretien, X. Qiu, Antiviral activity of quercetin-3-β-O-D-glucoside against Zika virus infection, Virol. Sin. 32 (2017) 545–547, https://doi.org/10.1007/s12250-017-4057-9.

[7] R.V. Patel, B.M. Mistry, S.K. Shinde, R. Syed, V. Singh, H.-S. Shin, Therapeutic potential of quercetin as a cardiovascular agent, Eur. J. Med. Chem. 155 (2018) 889–904, https://doi.org/10.1016/j.ejmech.2018.06.053.

[8] J. Wang, S. Geng, B. Wang, Q. Shao, Y. Fang, Y. Wei, Magnetic nanoparticles and high-speed countercurrent chromatography coupled in-line and using the same solvent system for separation of quercetin-3-O-rutinoside, luteoloside and astragalin from a Mikania micrantha extract, J. Chromatogr. A 1508 (2017) 42–52, https://doi.org/10.1016/j.chroma.2017.05.062.

[9] H. Wu, M. Chen, Y. Fan, F. Elsebaei, Y. Zhu, Determination of rutin and quercetin in Chinese herbal medicine by ionic liquid-based pressurized liquid extraction–liquid chromatography–chemiluminescence detection, Talanta 88 (2012) 222–229, https://doi.org/10.1016/j.talanta.2011.10.036.

[10] M. Rahimi, S. Bahar, R. Heydari, S.M. Amininasab, Determination of quercetin using a molecularly imprinted polymer as solid-phase microextraction sorbent and high-performance liquid chromatography, Microchem. J. 148 (2019) 433–441, https://doi.org/10.1016/j.microc.2019.05.032.

[11] M. Soylak, B. Ozdemir, E. Yilmaz, An environmentally friendly and novel amine-based liquid phase microextraction of quercetin in food samples prior to its determination by UV–vis spectrophotometry, Spectrochim. Acta Mol. Biomol. Spectrosc. 243 (2020) 118806, https://doi.org/10.1016/j.saa.2020.118806.

[12] A. Asfaram, M. Ghaedi, H. Javadian, A. Goudarzi, Cu- and S- @SnO2 nanoparticles loaded on activated carbon for efficient ultrasound assisted dispersive μSPE-spectrophotometric detection of quercetin in Nasturtium officinale extract and fruit juice samples: CCD-RSM design, Ultrason. Sonochem. 47 (2018) 1–9, https://doi.org/10.1016/j.ultsonch.2018.04.008.

[13] T.-Q. Song, K. Yuan, W.-Z. Qiao, Y. Shi, J. Dong, H.-L. Gao, X.-P. Yang, J.-Z. Cui, B. Zhao, Water stable [Tb $_4$ ] cluster-based metal–organic framework as sensitive and recyclable luminescence sensor of quercetin, Anal. Chem. 91 (2019) 2595–2599, https://doi.org/10.1021/acs.analchem.8b05281.

[14] A.F. Memon, A.R. Solangi, S.Q. Memon, A. Mallah, N. Memon, A.A. Memon, Simultaneous determination of quercetin, rutin, Naringin, and Naringenin in different fruits by capillary zone electrophoresis, Food Anal. Methods. 10 (2017) 83–91, https://doi.org/10.1007/s12161-016-0552-0.

[15] S. Xu, L. Chen, L. Ma, Fluorometric determination of quercetin by using graphitic carbon nitride nanoparticles modified with a molecularly imprinted polymer, Microchim. Acta 185 (2018) 492, https://doi.org/10.1007/s00604-018-3016-y.

[16] P. Zhao, M. Ni, Y. Xu, C. Wang, C. Chen, X. Zhang, C. Li, Y. Xie, J. Fei, A novel ultrasensitive electrochemical quercetin sensor based on MoS2 - carbon nanotube @ graphene oxide nanoribbons/HS-cyclodextrin/graphene quantum dots composite film, Sensor. Actuator. B Chem. 299 (2019) 126997, https://doi.org/10.1016/j.snb.2019.126997.

[17] M. Veerapandian, Y.-T. Seo, K. Yun, M.-H. Lee, Graphene oxide functionalized with silver@silica–polyethylene glycol hybrid nanoparticles for direct electrochemical detection of quercetin, Biosens. Bioelectron. 58 (2014) 200–204, https://doi.org/10.1016/j.bios.2014.02.062.

[18] S. Takahashi, H. Muguruma, N. Osakabe, H. Inoue, T. Ohsawa, Electrochemical determination with a long-length carbon nanotube electrode of quercetin glucosides in onion, apple peel, and tartary buckwheat, Food Chem. 300 (2019) 125189, https://doi.org/10.1016/j.foodchem.2019.125189.

[19] Z. Zhang, S. Gu, Y. Ding, M. Shen, L. Jiang, Mild and novel electrochemical preparation of β-cyclodextrin/graphene nanocomposite film for supersensitive sensing of quercetin, Biosens. Bioelectron. 57 (2014) 239–244, https://doi.org/10.1016/j.bios.2014.02.014.

[20] A. Chisvert, S. Cárdenas, R. Lucena, Dispersive micro-solid phase extraction, Trac. Trends Anal. Chem. 112 (2019) 226–233, https://doi.org/10.1016/j.trac.2018.12.005.

[21] M. Panagiotopoulou, S. Kunath, P.X. Medina-Rangel, K. Haupt, B. Tse Sum Bui, Fluorescent molecularly imprinted polymers as plastic antibodies for selective labeling and imaging of hyaluronan and sialic acid on fixed and living cells, Biosens. Bioelectron. 88 (2017) 85–93, https://doi.org/10.1016/j.bios.2016.07.080.

[22] J. O'Mahony, S. Wei, A. Molinelli, B. Mizaikoff, Imprinted polymeric materials. Insight into the nature of prepolymerization complexes of quercetin imprinted polymers, Anal. Chem. 78 (2006) 6187–6190, https://doi.org/10.1021/ac060446j.

[23] F. Canfarotta, A. Poma, A. Guerreiro, S. Piletsky, Solid-phase synthesis of molecularly imprinted nanoparticles, Nat. Protoc. 11 (2016) 443–455, https://doi.org/10.1038/nprot.2016.030.

[24] A. Lamaoui, A.A. Lahcen, J.J. García-Guzmán, J.M. Palacios-Santander, L. Cubillana-Aguilera, A. Amine, Study of solvent effect on the synthesis of magnetic molecularly imprinted polymers based on ultrasound probe: application for sulfonamide detection, Ultrason. Sonochem. 58 (2019) 104670, https://doi.org/10.1016/j.ultsonch.2019.104670.

[25] S. Sun, M. Zhang, Y. Li, X. He, A molecularly imprinted polymer with incorporated graphene oxide for electrochemical determination of quercetin, Sensors 13 (2013) 5493–5506, https://doi.org/10.3390/s130505493.

[26] M. Arabi, A. Ostovan, A.R. Bagheri, X. Guo, L. Wang, J. Li, X. Wang, B. Li, L. Chen, Strategies of molecular imprinting-based solid-phase extraction prior to chromatographic analysis, Trac. Trends Anal. Chem. 128 (2020) 115923, https://doi.org/10.1016/j.trac.2020.115923.
[27] M.T. Muldoon, L.H. Stanker, Molecularly imprinted solid phase extraction of atrazine from beef liver extracts, Anal. Chem. 69 (1997) 803–808, https://doi.org/10.1021/ac9604649.
[28] D. Li, T. Tu, M. Yang, C. Xu, Efficient preparation of surface imprinted magnetic nanoparticles using poly (2-anilinoethanol) as imprinting coating for the selective recognition of glycoprotein, Talanta 184 (2018) 316–324, https://doi.org/10.1016/j.talanta.2018.03.012.
[29] G. Goyal, S. Bhakta, P. Mishra, Surface molecularly imprinted biomimetic magnetic nanoparticles for enantioseparation, ACS Appl. Nano Mater. 2 (2019) 6747–6756, https://doi.org/10.1021/acsanm.9b01649.
[30] A. Lamaoui, L. Cubillana-Aguilera, M.L.A. Gil, A. Amine, J.M. Palacios-Santander, Chapter 16. Analytical applications of molecularly imprinted polymer-decorated magnetic nanoparticles, in: C.M. Hussain (Ed.), Analytical Applications of Functionalized Magnetic Nanoparticles, Royal Society of Chemistry, Cambridge, 2021, pp. 397–428, https://doi.org/10.1039/9781839162756-00397.
[31] M. Kharroubi, F. Bellali, A. Karrat, M. Bouchdoug, A. Jaouad, Preparation of *Teucrium polium* extract-loaded chitosan-sodium lauryl sulfate beads and chitosan-alginate films for wound dressing application, AIMSPH 8 (2021) 754–775, https://doi.org/10.3934/publichealth.2021059.
[32] A. Karrat, A. Lamaoui, A. Amine, J.M. Palacios-Santander, L. Cubillana-Aguilera, Applications of chitosan in molecularly and ion imprinted polymers, Chem. Afr. 3 (2020) 513–533, https://doi.org/10.1007/s42250-020-00177-w.
[33] M.A. Kafi, A. Paul, A. Vilouras, R. Dahiya, Mesoporous chitosan based conformable and resorbable biostrip for dopamine detection, Biosens. Bioelectron. 147 (2020) 111781, https://doi.org/10.1016/j.bios.2019.111781.
[34] A. Lamaoui, J.J. García-Guzmán, A. Amine, J.M. Palacios-Santander, L. Cubillana-Aguilera, Synthesis techniques of molecularly imprinted polymer composites, in: Molecularly Imprinted Polymer Composites, Elsevier, 2021, pp. 49–91, https://doi.org/10.1016/B978-0-12-819952-7.00002-0.
[35] M. Sher, R. Zhuang, U. Demirci, W. Asghar, Paper-based analytical devices for clinical diagnosis: recent advances in the fabrication techniques and sensing mechanisms, Expert Rev. Mol. Diagn. 17 (2017) 351–366, https://doi.org/10.1080/14737159.2017.1285228.
[36] O. El hani, A. Karrat, K. Digua, A. Amine, Development of a simplified spectrophotometric method for nitrite determination in water samples, Spectrochim. Acta Mol. Biomol. Spectrosc. 267 (2021), 120574, https://doi.org/10.1016/j.saa.2021.120574.
[37] L. Liu, L. Xiao, H. Zhu, X. Shi, Preparation of magnetic and fluorescent bifunctional chitosan nanoparticles for optical determination of copper ion, Microchim. Acta 178 (2012) 413–419, https://doi.org/10.1007/s00604-012-0855-9.
[38] A. Karrat, A. Amine, Solid-phase extraction combined with a spectrophotometric method for determination of Bisphenol-A in water samples using magnetic molecularly imprinted polymer, Microchem. J. 168 (2021) 106496, https://doi.org/10.1016/j.microc.2021.106496.
[39] Z. Chen, X. Wang, Y. Chen, Z. Xue, Q. Guo, Q. Ma, H. Chen, Preparation and characterization of a novel nanocomposite with double enzymes immobilized on magnetic Fe 3 O 4 -chitosan-sodium tripolyphosphate, Colloids Surf. B Biointerfaces 169 (2018) 280–288, https://doi.org/10.1016/j.colsurfb.2018.04.066.
[40] Y. Hong, L. Chen, Extraction of quercetin from Herba Lysimachiae by molecularly imprinted-matrix solid phase dispersion, J. Chromatogr. B 941 (2013) 38–44, https://doi.org/10.1016/j.jchromb.2013.10.002.
[41] V. Pakade, S. Lindahl, L. Chimuka, C. Turner, Molecularly imprinted polymers targeting quercetin in high-temperature aqueous solutions, J. Chromatogr. A 1230 (2012) 15–23, https://doi.org/10.1016/j.chroma.2012.01.051.
[42] A. Asfaram, M. Arabi, A. Ostovan, H. Sadeghi, M. Ghaedi, Simple and selective detection of quercetin in extracts of plants and food samples by dispersive-micro-solid phase extraction based on core–shell magnetic molecularly imprinted polymers, New J. Chem. 42 (2018) 16144–16153, https://doi.org/10.1039/C8NJ03349H.
[43] C. Wang, Y. Zuo, Ultrasound-assisted hydrolysis and gas chromatography–mass spectrometric determination of phenolic compounds in cranberry products, Food Chem. 128 (2011) 562–568, https://doi.org/10.1016/j.foodchem.2011.03.066.
[44] S.-P. Wang, K.-J. Huang, Determination of flavonoids by high-performance liquid chromatography and capillary electrophoresis, J. Chromatogr. A 1032 (2004) 273–279, https://doi.org/10.1016/j.chroma.2003.11.099.
[45] M. Hassan, F. Uzcan, S.N. Shah, U. Alshana, M. Soylak, Switchable-hydrophilicity solvent liquid-liquid microextraction for sample cleanup prior to dispersive magnetic solid-phase microextraction for spectrophotometric determination of quercetin in food samples, Sustain. Chem. Pharm. 22 (2021) 100480, https://doi.org/10.1016/j.scp.2021.100480.
[46] R. Khani, R. Sheykhi, G. Bagherzade, An environmentally friendly method based on micro-cloud point extraction for determination of trace amount of quercetin in food and fruit juice samples, Food Chem. 293 (2019) 220–225, https://doi.org/10.1016/j.foodchem.2019.04.099.
[47] M. Katyal, Analytical reactions of hydroxyflavones, Talanta 24 (1977) 367–375, https://doi.org/10.1016/0039-9140(77)80022-2.
[48] A. Michalkiewicz, M. Biesaga, K. Pyrzynska, Solid-phase extraction procedure for determination of phenolic acids and some flavonols in honey, J. Chromatogr. A 1187 (2008) 18–24, https://doi.org/10.1016/j.chroma.2008.02.001.
[49] V.E. Pakade, E.D. Molefe, N.T. Tavengwa, Quantitative determination of trace concentrations of quercetin from prickly pear skin complex sample extracts by application of molecularly imprinted polymers, J. Environ. Chem. Eng. 5 (2017) 1186–1195, https://doi.org/10.1016/j.jece.2017.01.051.
[50] T. Asadollahi, S. Dadfarnia, A.M. Haji Shabani, M. Amirkavei, Separation/preconcentration and determination of quercetin in food samples by dispersive liquid–liquid microextraction based on solidification of floating organic drop -flow injection spectrophotometry, J. Food Sci. Technol. 52 (2015) 1103–1109, https://doi.org/10.1007/s13197-013-1077-9.